ARTICLE NO. 79-1549R

J80-209

Numerical Simulation of Multistream Nozzle Flows

K. M. Peery* and C. K. Forester*
Boeing Aerospace Company, Seattle, Wash.

Numerical simulations are presented for steady multistream nozzle flows, including the flowfield of a scale model turbofan nozzle installation with transonic external flow. Steady-state solutions to the Navier-Stokes equations are obtained using a time dependent method by MacCormack. Wall functions and mesh fitting are utilized for improved computational efficiency. Favorable agreement is shown between computed and measured surface static pressure distributions. The effects of the internal fan duct and the external fan cowl boundary-layer velocity profiles upon the nozzle flowfield are shown to be very significant.

Nomenclature

C_V = specific heat capacity at constant volume
C = sonic velocity
e = specific internal energy
E = total energy density
M = Mach number
$\bar{n}$ = unit normal vector
NPR = nozzle pressure ratio
P = pressure
$\bar{q}$ = total velocity vector
R = gas constant
S = surface area
t = time
Δt = time increment
T = absolute temperature
u,v = Cartesian velocity components
vol = cell volume
V = volume
x,y,z = Cartesian coordinates
ρ = density
λ = second viscosity coefficient
κ = von Kármán constant = 0.41
η = distance coordinate, normal to wall
τ_{xy} = shear stress
σ_x,σ_y = normal stresses
μ_ℓ = laminar viscosity coefficient
μ_t = turbulent eddy viscosity coefficient

Subscripts

i,j = cell indices
t = total thermodynamic state
∞ = freestream

Introduction

THE design of jet engine exhaust nozzle installations requires gross performance measures such as drag, structural loads on nozzle components, thrust, and the discharge flowrate to evaluate candidate nozzle configurations on the basis of airplane mission performance. As shown in Fig. 1, a typical three-stream nozzle flowfield (two supersonic jets and one subsonic external stream) contains mixed subsonic and supersonic regions in which shocks and strong compression and expansion waves interact with boundary layers, mixing layers, and regions of separated flow. Because of the extreme complexity of the nozzle flowfield the designer traditionally uses model scale parametric testing to build a data base from which the full scale nozzle performance can be predicted. This process is usually iterated with full scale testing for validation and optimization until a satisfactory design is achieved.

The traditional test based approach to nozzle design is slow, uncertain, and expensive. These disadvantages have created considerable interest in developing analytical procedures for simulating nozzle flows. Currently, the state-of-the-art for numerically simulating nozzle flows is such that the designer can use existing analyses to supplement and guide his parametric test program. As computer capabilities increase and numerical algorithms become more sophisticated, numerical flow analysis will play an ever greater role in nozzle design. Parametric analysis will gradually replace parametric testing in the design process and eventually, only testing to validate the chosen design will be required.

One generally successful technique for computing steady state nozzle flowfields is to solve the governing unsteady flow equations using a finite difference approximation by marching in time to steady state. Using this approach, Serra,[1] Wehofer and Moger,[2] Migdal et al.,[3] Prozan et al.,[4] and, more recently, Cline[5] have solved the two-dimensional inviscid Euler equations for single-stream nozzle flows. Those researchers used body fitted computational meshes to ease application of boundary conditions. Free jet plumes were computed by both Wehofer and Moger, and Cline. Cline[6] extended the analysis to include viscous effects by using the same technique to solve the two-dimensional Navier-Stokes equations. Parathasarathy and Bozzola[7] computed a two-stream inviscid nozzle flowfield in which the computational mesh was fitted to the common streamline between the two supersonic streams. Mikhail et al.[8] have recently obtained steady-state solutions to the two-dimensional Navier-Stokes equations for supersonic flow over a conical convergent nozzle with supersonic jet. Using a time dependent method Holst[9] obtained steady-state solutions to the Navier-Stokes equations for viscous flows over nozzle boattails with

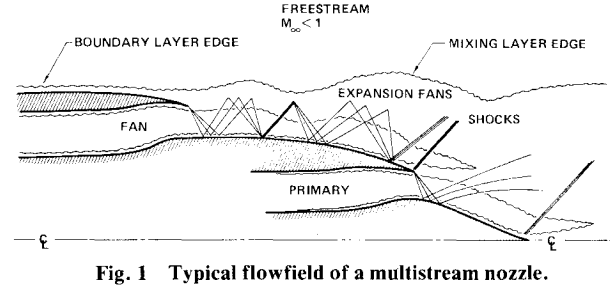

Fig. 1 Typical flowfield of a multistream nozzle.

Presented as Paper 79-1549 at the AIAA 12th Fluid and Plasma Dynamics Conference, Williamsburg, Va., July 23-25, 1979; submitted Oct. 1, 1979; revision received Feb. 20, 1980.

Index categories: Nozzle and Channel Flow; Transonic Flow; Airbreathing Propulsion.

*Research Engineer.

shock/boundary-layer interactions and a grossly separated boundary layer. The jet plume was simulated by a solid cylindrical core and the freestream was supersonic. An analysis for computing three-stream viscous nozzle flows with subsonic or transonic external streams has not yet been reported. Nozzle installations with three streams are presently and will continue to be of interest for commercial and military aircraft.

A computational procedure has been developed for simulating steady two-dimensional (planar or axisymmetric) nozzle flowfields with up to three conflowing fluid streams of arbitrary flow speed. The MacCormack finite difference algorithm[10] is used for solving the discretized Navier-Stokes equations. An important application of the procedure is the computation of a three-stream turbofan jet engine nozzle flow with a transonic external stream. Initial work was reported by Forester.[11]

The analysis and computed results for three nozzle configurations are presented. These results demonstrate the applicability of the analysis to a wide range of nozzle and freestream conditions. The analysis is validated through comparison of computed results with experimental data and, where applicable, to solutions by the method of characteristics.[12] Model scale and full scale numerical simulations of a JT9D turbofan engine nozzle flow with a transonic external stream are used to illustrate the traditional difficulty in scaling model scale nozzle test results (with a transonic freestream) to full scale.

Analysis

Governing Equations

The unsteady two-dimensional Navier-Stokes equations for the turbulent flow of a nonconducting fluid with negligible viscous dissipation can be written in integral form for a fluid volume V bounded by the surface S.

$$\frac{\partial}{\partial t}\int_V \bar{U}\,dV+\int_S \bar{\bar{H}}\cdot\bar{n}\,dS=0 \tag{1}$$

The Cartesian vector $\bar{U}$ and the second order Cartesian tensor $\bar{\bar{H}}$ are defined as

$$\bar{U}=\begin{Bmatrix}\rho\\ \rho u\\ \rho v\\ E\end{Bmatrix} \qquad \bar{\bar{H}}=\begin{Bmatrix}\rho u & \rho v\\ \rho u^2+\sigma_x & \rho uv+\tau_{xy}\\ \rho uv+\tau_{yx} & \rho v^2+\sigma_y\\ (E+P)u & (E+P)v\end{Bmatrix}$$

where the total energy density E is defined as

$$E=\rho[e+\tfrac{1}{2}(u^2+v^2)]$$

The stress components are defined as

$$\sigma_x=P-\lambda\left(\frac{\partial u}{\partial x}+\frac{\partial v}{\partial y}\right)-2\mu\frac{\partial u}{\partial x}$$

$$\sigma_y=P-\lambda\left(\frac{\partial u}{\partial x}+\frac{\partial v}{\partial y}\right)-2\mu\frac{\partial v}{\partial y}$$

$$\tau_{xy}=\tau_{yx}=-\mu\left(\frac{\partial u}{\partial y}+\frac{\partial v}{\partial x}\right)$$

$$\lambda=-\tfrac{2}{3}\mu \qquad \mu=\mu_\ell+\mu_t$$

To achieve closure to the set of governing equations, a turbulence model that relates the Reynolds stress components to the mean flow is required. Details of the turbulence models used in the analysis are given in the Results and Discussion section.

The fluid is air with ideal gas behavior. The ratio of specific heat capacities is 1.4 and the gas constant is 287 J/kg-K.

$$P=\rho RT \qquad e=C_vT$$

Difference Equations

The governing equations are solved using the explicit predictor-corrector finite difference algorithm of MacCormack[13,14] in conservation law form for a nonorthogonal body fitted computational mesh. The split finite difference operators, which advance the solution from the n time level to the $n+1$ time level, are given below for two-dimensional planar flow.

$$\bar{U}_{i,j}^{n+1}=LI(\Delta t)\;LJ(\Delta t)\;\bar{U}_{i,j}^{n} \tag{2}$$

The $LJ\;(\Delta t)$ operator is defined as

$$\bar{U}_{i,j}^{n+\frac{1}{2}}=\bar{U}_{i,j}^{n}-\frac{\Delta t}{\mathrm{vol}_{i,j}}\left[\bar{\bar{H}}_{i,j}^{n}\cdot\bar{S}_3+\bar{\bar{H}}_{i,j-1}^{n}\cdot\bar{S}_1\right]$$

$$\bar{U}_{i,j}^{n+\frac{1}{2}}=\tfrac{1}{2}\left(\bar{U}_{i,j}^{n}+\bar{U}_{i,j}^{n+\frac{1}{2}}-\frac{\Delta t}{\mathrm{vol}_{i,j}}\left[\bar{\bar{H}}_{i,j+1}^{n+\frac{1}{2}}\cdot\bar{S}_3+\bar{\bar{H}}_{i,j}^{n+\frac{1}{2}}\cdot\bar{S}_1\right]\right)$$

and the $LI\;(\Delta t)$ operator is defined as

$$\bar{U}_{i,j}^{n+1}=\bar{U}_{i,j}^{n+\frac{1}{2}}-\frac{\Delta t}{\mathrm{vol}_{i,j}}\left[\bar{\bar{H}}_{i,j}^{n+\frac{1}{2}}\cdot\bar{S}_4+\bar{\bar{H}}_{i-1,j}^{n+\frac{1}{2}}\cdot\bar{S}_2\right]$$

$$\bar{U}_{i,j}^{n+1}=\tfrac{1}{2}\left(\bar{U}_{i,j}^{n+\frac{1}{2}}+\bar{U}_{i,j}^{n+1}-\frac{\Delta t}{\mathrm{vol}_{i,j}}\left[\bar{\bar{H}}_{i+1,j}^{n+1}\cdot\bar{S}_4+\bar{\bar{H}}_{i,j}^{n+1}\cdot\bar{S}_2\right]\right)$$

The superscripts denote the time level, $t=n\Delta t$. Subscripts i and j denote the spatial location of the cell centered field variables in the computational mesh. The scheme is second-order accurate in space, but since the operators are not applied symmetrically, it is only first-order accurate in time. However, only steady-state solutions are of interest, therefore the lack of operator symmetry is acceptable.

In planar two-dimensional calculations the cells are of uniform unit depth (in the Z direction), and the cell faces in the x-y plane are general quadrilaterals. A typical mesh cell is shown in Fig. 2a. The vector $\bar{S}_i$ is equal to $\bar{n}_iS_i$, where $\bar{n}_i$ is the outward directed unit normal vector and S_i is the area of the ith cell face.

Axisymmetric solutions are obtained with the equations above using the Cartesian dependent and independent variables with the following modifications. The cell depth

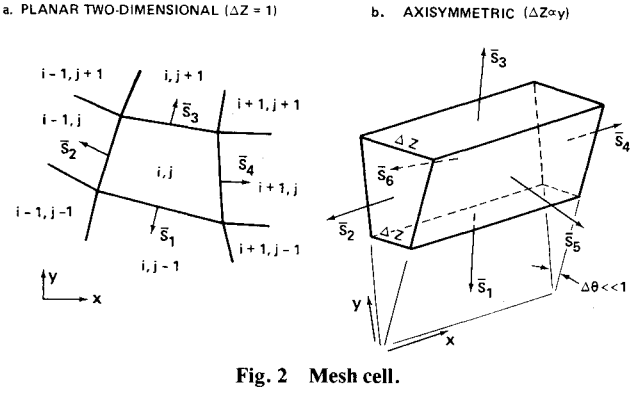

Fig. 2 Mesh cell.

(Δz) is made proportional to the Cartesian coordinate y, as shown in Fig. 2b. An additional normal stress (σ_y) which acts upon cell surfaces S_5 and S_6, also shown in Fig. 2b, is included in the set of difference equations in a manner similar to the way pressure is treated in variable area one-dimensional gas dynamics equations. Shear stresses acting on surfaces S_5 and S_6 are estimated to be small in comparison to σ_y, and are therefore neglected. Since $\Delta\theta$ (see Fig. 2b) is made arbitrarily small, axisymmetric solutions result, where y corresponds to the radial position coordinate and v corresponds to the radial velocity component.

Derivatives required to evaluate the stress components are obtained by a transformation to a nonorthogonal coordinate system associated with the mesh lines. Details of this transformation are given by Deiwert.[15]

The time step must satisfy the following stability conditions.

$$\Delta t = \min\left\{ \mathrm{vol}_{i,j} \Big/ \left[\bar{q}_{i,j} \cdot \bar{S}_4 + C_{i,j} (\bar{S}_4 \cdot \bar{S}_4)^{1/2} + 2 \frac{\mu_{i,j} (\bar{S}_4 \cdot \bar{S}_4)}{\rho_{i,j} \mathrm{vol}_{i,j}} \right] \right\}$$

and

$$\Delta t = \min\left\{ \mathrm{vol}_{i,j} \Big/ \left[\bar{q}_{i,j} \cdot \bar{S}_3 + C_{i,j} (\bar{S}_3 \cdot \bar{S}_3)^{1/2} + 2 \frac{\mu_{i,j} (\bar{S}_3 \cdot \bar{S}_3)}{\rho_{i,j} \mathrm{vol}_{i,j}} \right] \right\}$$

For the calculations reported, the time steps of each operator were approximately 0.9 times the maximum time step allowed by the stability conditions above.

In Ref. 14 the volumetric flux between two cells within an expansion region of the flow was calculated by averaging the two cell centered velocities. The stated purpose of this was to prevent a nonlinear numerical instability. The convergence rate of the present analysis with this velocity averaging process was found to be severely retarded and was therefore not used. This behavior is attributed to the amplification of small amplitude pressure waves by the switching on and off of the velocity averaging process.

Smoothing Terms

In regions of low fluid velocity and particularly regions where there exist large second derivatives in the conservative field variables, the algorithm requires additional smoothing to prevent numerical instability. Explicit smoothers are used in the present analysis similar to the fourth-order pressure terms introduced by MacCormack[14] and three point second-order diffusion.

Boundary Conditions

In the present analysis boundary conditions are imposed using fictitious cells bordering the computational mesh. At solid impermeable boundaries convection terms are explicitly zeroed to maintain strict mass conservation and a zero normal pressure gradient is assumed. Velocity components are reflected at free-slip surfaces and wall functions are used at viscous no-slip surfaces. Total pressure, total temperature, and flow angle are specified at subsonic inflow boundaries with the remaining field variables obtained by assuming a zero axial gradient in each variable. At supersonic inflow boundaries all field variables are prescribed. Linear extrapolation is used for all field variables at purely supersonic outflow boundaries. Planes and axes of symmetry are treated as solid free-slip boundaries.

For multistream nozzle calculations, where both subsonic and supersonic flow occurred at the outflow boundary, the freestream static pressure is prescribed at each cell regardless of the local Mach number. The remaining field variables are obtained by assuming a zero axial gradient in each variable. A shock or sudden expansion wave is predicted at the outflow boundary where the flow at the boundary is supersonic, but since these disturbances do not propagate upstream, their presence has little effect upon the computed solution over four cells away from the boundary.

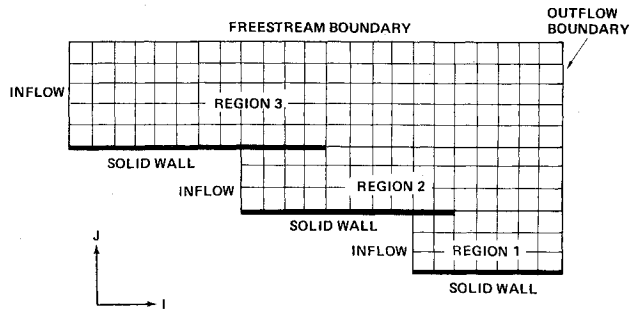

Fig. 3 Computational domain, *I-J* space.

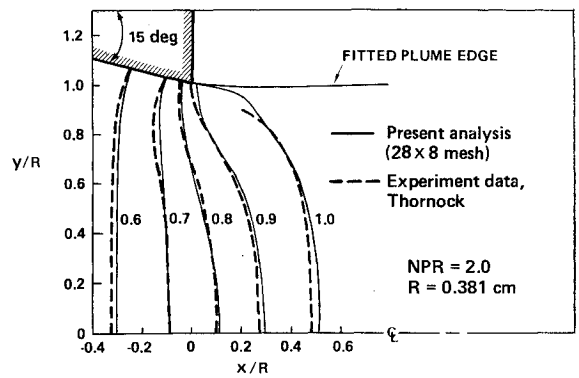

Fig. 4 Mach number contours – 15 deg conical nozzle.

Wall Functions

Resolution of turbulent boundary layers requires a very fine computational mesh near the solid boundaries. The stability condition described above requires an exceedingly small time step size. This drives the computation time prohibitively large for practical nozzle design calculations. In the present analysis wall functions as described by Launder and Spalding[16] are used to obtain the wall shear stresses and convective fluxes in the mesh cells bordering solid boundaries. This greatly reduces the mesh required for boundary layers.

Initial Conditions

The field variables are initialized using the one-dimensional gas dynamic equations. The initial velocity vector field is adjusted so that the flow is tangent to the nozzle surfaces.

Mesh Generation and Mesh Fitting

Up to three mesh regions are generated; one for each fluid stream. In the *I-J* logic space each region is rectangular and has a separate *I-J* indexing scheme as shown in Fig. 3. *I*-mesh lines are vertical and parallel to the y coordinate axis and *J*-mesh lines are fitted to the nozzle surfaces.

Fitting a computational mesh to flowfield discontinuities (e.g., shocks and slip surfaces) has been shown to reduce the generation of computational noise.[17,18] Fitting can also be used to position fine mesh for resolving thin mixing layers between fluid streams. These benefits result in efficient use of available mesh.

During the calculation the y coordinates of cell vertices on mesh lines between mesh regions are continually and automatically moved according to the transport equation.

$$\frac{\partial Y}{\partial t} = \beta\left(\hat{v} - \hat{u}\frac{\partial Y}{\partial x}\right)$$

Y is the y coordinate of the mesh cell vertex, $\hat{u}$ and $\hat{v}$ are simple averages of local cell centered velocity components, and β is a damping coefficient. With upwind differencing for $\partial Y/\partial x$, forward differencing for $\partial Y/\partial t$, and $\beta = 0.1$ the scheme is stable. At steady state the mesh is aligned with the dividing streamlines between the fluid streams. The other J-mesh lines are periodically adjusted to conform to the fitted mesh lines, thus avoiding large differences in neighboring cell volumes. Since the fluxes across the fitted mesh are not modified to account for the mesh velocity, the scheme is not time accurate. The transport equation is also used to move the computational mesh so that it conforms to an inviscid jet plume boundary for calculating single-stream nozzle flows. In this case, $\hat{u}$ and $\hat{v}$ are averaged from the two neighboring cells below each cell vertex.

Results and Discussion

Calculated results are presented for three different nozzle configurations: 1) a single-stream, 15 deg convergent conical nozzle, 2) a two-stream, two-dimensional wedge plug nozzle, and 3) a three-stream scale-model turbofan jet engine exhaust nozzle. Computing times quoted for the following calculations are for execution on a Control Data Corp. Cyber 175 computer. A convergence parameter was defined as the maximum fractional change of static pressure per time step in the mesh. Computed results and detailed discussion of how the analysis was applied for each case follows.

Conical Nozzle

The steady-state flowfield of an axisymmetric 15 deg convergent conical nozzle was computed in a mesh of 28×8 cells for a nozzle pressure ratio of 2.0 and total temperature of 355.5 K. Viscous terms were set equal to zero to obtain an Euler equations solution. The mesh was fitted to the plume boundary, where the ambient static pressure was prescribed. Calculated Mach number contours, shown in Fig. 4, compare well with experimental data by Thornock.[19] The convergence characteristics of the calculation are shown in Fig. 5. Approximately 800 time steps and 40 s of CPU time were required to reduce the convergence parameter below 0.001.

Two-Dimensional Wedge Plug Nozzle

The analysis was used to compute the inviscid steady-state flowfield of the two-dimensional wedge plug nozzle shown in Fig. 6. Three calculations were made at freestream Mach numbers of 0.0, 0.9, and 2.0 at a nozzle pressure ratio of 5. The total temperature in the jet stream was 300 K. The static temperature of the freestream was 300 K. Two mesh regions were required. The inner jet mesh consisted of 50×10 cells. The external mesh was 56×26 cells and was stretched exponentially 77.5 nozzle heights (H, see Fig. 6) away from the nozzle. In addition the external mesh was exponentially stretched upstream approximately 10 nozzle heights from the trailing edge of the cowl. The mesh extended downstream approximately 5.5 nozzle heights. At steady state the mesh has aligned with the dividing streamline between the two regions as shown in Fig. 7.

Computed Mach number contours for the three cases are shown in Fig. 8. Computed surface static pressures are shown in Fig. 9. Essentially exact solutions to the Euler equations for this problem were obtained for the static freestream ($M_\infty = 0$) and supersonic freestream ($M_\infty = 2$) cases using a method of characteristics computer code.[12] The surface static pressures computed with the present analysis shown in Fig. 10 are in good agreement with those calculated by the method of characteristics. Computing times for these calculations were between 10 and 15 min to achieve a convergence level less than 10^{-2}.

Scale Model JT9D

The flowfield was calculated in and around a 1/22 scale model nozzle of a JT9D turbofan jet engine as shown schematically in Fig. 11 at a nozzle pressure ratio of 2.62 (both fan and primary jets) for a freestream Mach number of 0.9. A thick boundary layer (approximately 1.5 cm) existed on the outer fan cowl surface. The fan jet and primary jet were supplied with unheated air at a total temperature of about 300 K through long ducts inside the sting supporting the model in the wind tunnel. Detailed measurements of flow conditions upstream of the fan duct nozzle were not available, although averaged conditions were known. Because of the long annular duct (over 50 annular heights long) a fully developed turbulent profile was assumed entering the fan nozzle in order to determine the boundary conditions for this calculation. A perforated choke plate was located upstream of the primary nozzle. This resulted in an approximately uniform total pressure profile in the flow entering the primary nozzle.

Three algebraic eddy viscosity turbulence models (models A, B, and C) were patched together as shown in Fig. 12. Model A was a two-layer mixing length model. In the inner region

$$\mu_t = \rho(\kappa\eta)^2 \left| \frac{\partial u}{\partial y} \right|$$

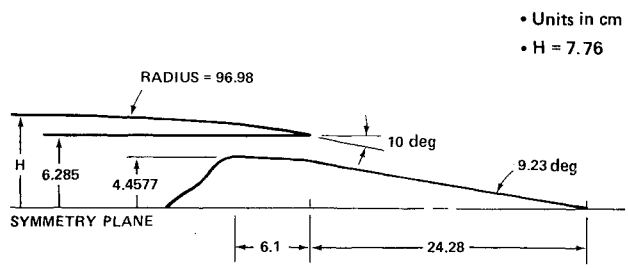

Fig. 6 Wedge plug nozzle geometry.

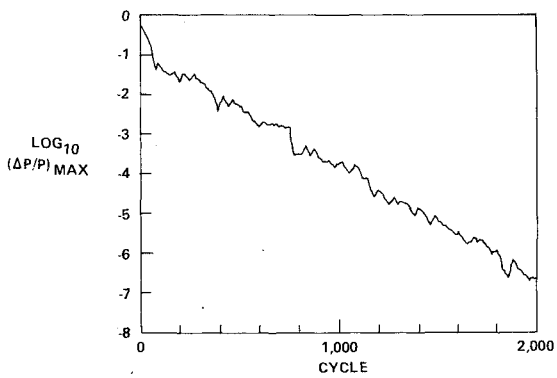

Fig. 5 Convergence history – 15 deg conical nozzle.

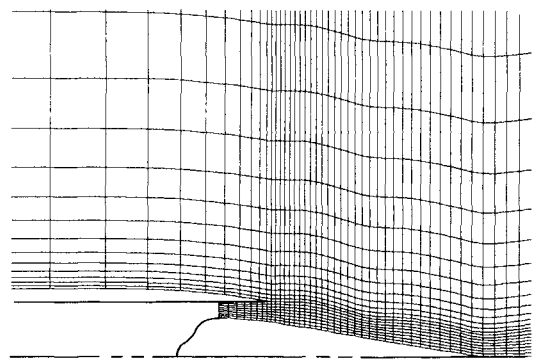

Fig. 7 Wedge plug nozzle mesh at steady state, $M_\infty = 0$.

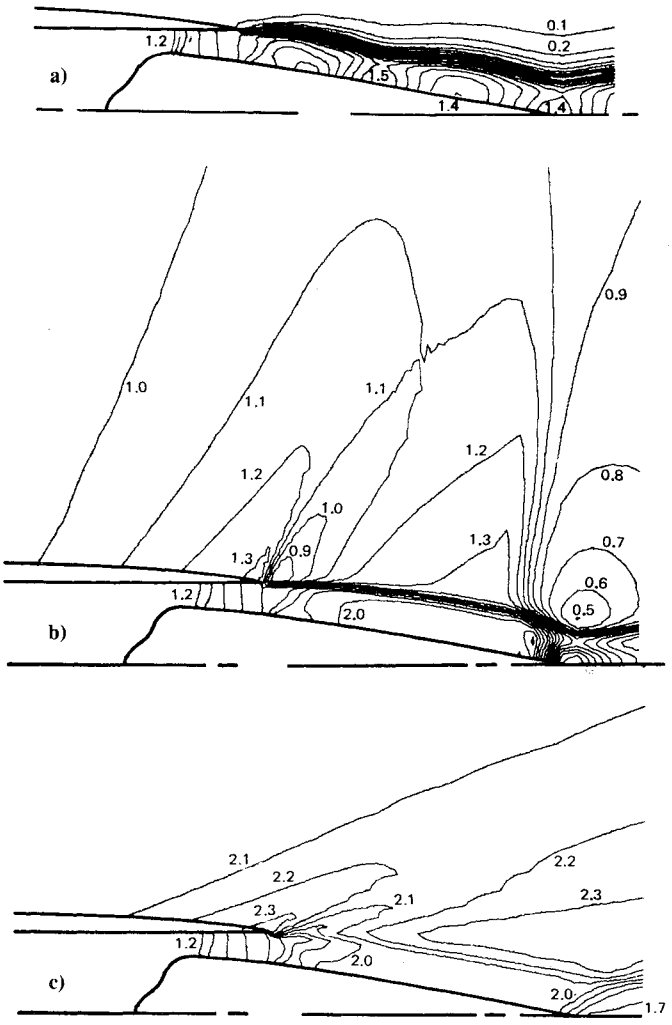

Fig. 8 Wedge plug nozzle Mach number contours; a) $M_\infty = 0.0$, b) $M_\infty = 0.9$, and c) $M_\infty = 2.0$.

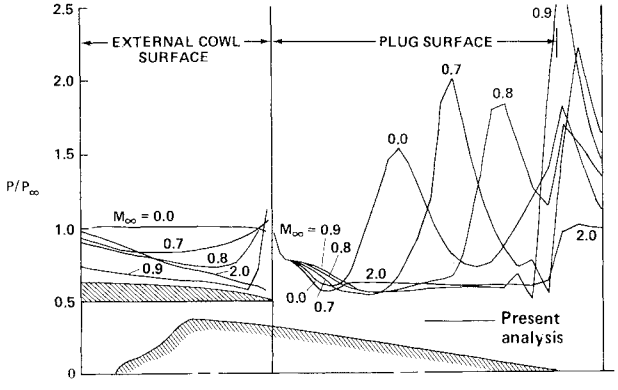

Fig. 9 Wedge plug nozzle surface static pressure.

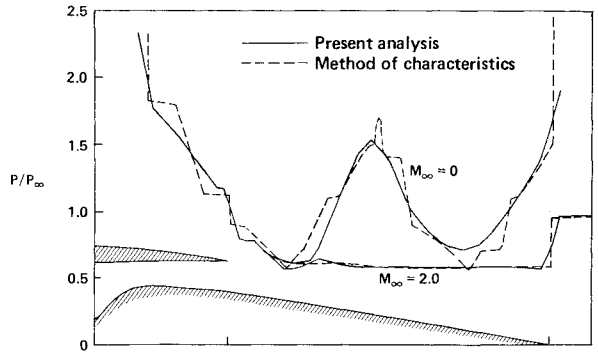

Fig. 10 Wedge plug nozzle static pressure on plug surface.

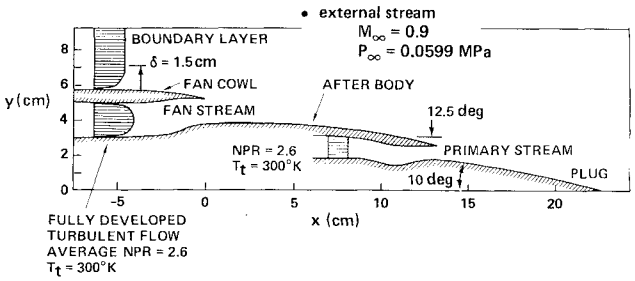

Fig. 11 JT9D scale-model nozzle geometry.

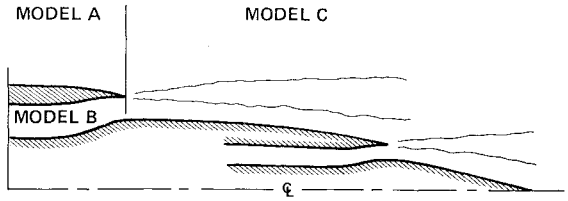

Fig. 12 Zonal turbulence models for JT9D scale-model calculation.

where η is the distance normal to the wall. In the outer region

$$\mu_t = \rho(0.09\delta)^2 \left| \frac{\partial u}{\partial y} \right|$$

where δ is the boundary layer thickness. At points within the boundary layer both the inner and outer values of μ_t were computed and the minimum value was used. In model B the eddy viscosity was computed from the following mixing length formula:

$$\mu_t = \rho \ell^2 \left| \frac{\partial u}{\partial y} \right|$$

Since the flow in the fan duct was estimated to be turbulent and fully developed, the mixing length ℓ was approximated by the Nikuradse formula[20] for the mixing length in fully developed turbulent pipe flow. The computed length of the internal fan duct flow was of such a short distance the effects of viscosity upon the bulk of the fan duct flow in that region was minimal. Therefore, this simple model was deemed adequate, particularly in view of the uncertainty relating to the upstream fan duct flow conditions. Model C, used in the mixing layer regions, is a simple mixing length model where the eddy viscosity is computed by

$$\mu_t = 0.017 \rho L |\Delta \tilde{u}|$$

where L is the thickness of the mixing layer and $\Delta\tilde{u}$ the difference between the tangential velocities across the layer. The mixing layer thickness was assumed to vary linearly with downstream distance having an initial value (L_0) equal to the outer cowl boundary layer thickness. Where x_0 is the axial location of the cowl trailing edge,

$$L = 0.12(x - x_0) + L_0$$

The flowfield of the scale model JT9D nozzle was discretized using a mesh of 2765 cells. The mesh was ex-

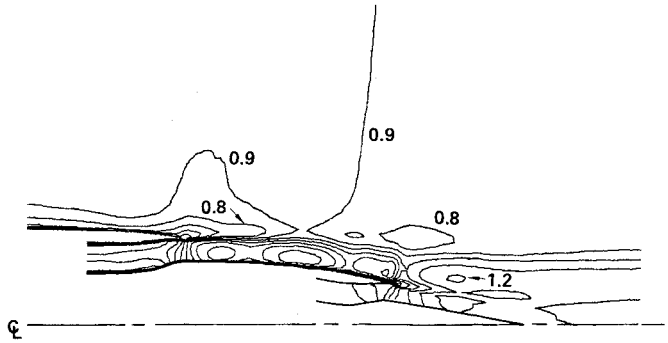

Fig. 13 JT9D scale-model nozzle Mach number contours.

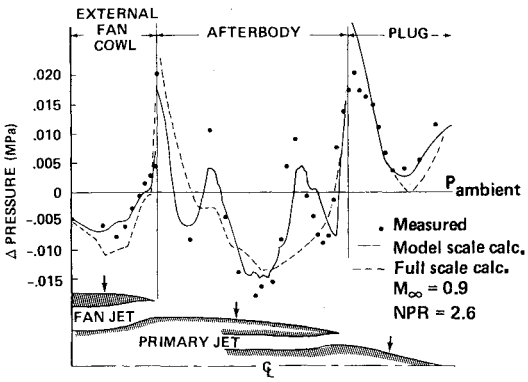

Fig. 14 JT9D scale-model nozzle surface static pressures.

ponentially stretched upstream from the fan cowl trailing edge approximately five nozzle diameters. The outflow boundary was positioned approximately one nozzle diameter downstream of the nozzle plug tip. Waves evident in these meshes result from the alignment of the mesh with the two dividing streamlines between the three fluid streams.

The computed Mach number contours are shown in Fig. 13. The computed static pressures on the three external surfaces of the nozzle are compared to measured pressures[21] in Fig. 14. Considering the uncertainty related to the fan duct upstream flow conditions the agreement between calculated and measured values is good.

In simulating nozzle flows, either numerically, by full scale testing, or by model scale testing, attention should be addressed to correctly imposing or identifying upstream flow conditions. To illustrate the effect of the outer fan cowl boundary layer and the fan duct total pressure profile upon the nozzle afterbody pressure distribution, a second calculation is presented in which free-slip conditions were set on all nozzle surfaces. A uniform total pressure profile was prescribed at the fan duct inflow boundary, having the same area averaged total pressure as the previous calculation. Uniform total pressure profiles were prescribed at the inflow boundaries of the external stream and the primary jet stream. These changes approximate a full scale nozzle flow, where in relation to nozzle geometry, the boundary layers would be much smaller than in model scale. The static pressure distribution on the nozzle surfaces for this calculation is compared with the model scale results in Fig. 14. Significant differences are shown between the two calculations indicating the importance of correctly simulating upstream conditions.

CPU time required for a given JT9D calculation was approximately 30 min, where the convergence parameter was less than 10^{-5}.

Conclusions

The present computational procedure has successfully been used for the numerical simulation of the steady viscous flow of a three-stream nozzle in which the external stream was transonic. The procedure is applicable to the calculation of multistream nozzle flows with static, subsonic, transonic, and supersonic external streams.

The importance of correctly accounting for upstream flow conditions when simulating nozzle flows, either numerically or by model scale test, has been demonstrated using the computational procedure.

References

[1] Serra, R.A., "Determination of Internal Gas Flows by a Transient Numerical Technique," *AIAA Journal,* Vol. 10, May 1972, pp. 603-611.

[2] Wehofer, S. and Moger, W.C., "Transonic Flow in Conical Convergent and Convergent-Divergent Nozzles with Nonuniform Inlet Conditions," AIAA Paper 70-635, June 1970.

[3] Migdal, D., Klein, K., and Moretti, G., "Time-Dependent Calculations for Transonic Nozzle Flow," *AIAA Journal,* Vol. 7, Feb. 1969, pp. 372-374.

[4] Prozan, R.J., Spradley, L.W., Anderson, P.G., and Pearson, M.L., "The General Interpolants Method: A Procedure For Generating Numerical Analogs of the Conservation Laws," AIAA Paper 77-642, June 1977.

[5] Cline, M.C., "Computation of Steady Nozzle Flow by a Time-Dependent Method," *AIAA Journal,* Vol. 12, April 1974, pp. 419-420.

[6] Cline, M.C., "Computation of Two-Dimensional, Viscous Nozzle Flow," *AIAA Journal,* Vol. 14, March 1976, pp. 295-296.

[7] Parathasarathy, K. and Bozzola, R., "The Computation of Steady Exhaust Nozzle Flows By a Time Dependent Method," AIAA Paper 76-151, Jan. 1976.

[8] Mikhail, A.G., Hankey, W.L., and Shang, J.S., "Computation of a Supersonic Flow Past an Axisymmetric Nozzle Boattail with Jet Exhaust," AIAA Paper 78-993, July 1978.

[9] Holst, T.L., "Numerical Solution of Axisymmetric Boattail Flow Fields with Plume Simulators," AIAA Paper 77-224, Jan. 1977.

[10] MacCormack, R.W. and Paullay, A.J., "Computational Efficiency Achieved by Time Splitting of Finite Difference Operators," AIAA Paper 72-154, Jan. 1972.

[11] Forester, C.K., "Numerical Simulation of the Interaction of Jet and Freestream Flows in Engine Exhaust Systems," AIAA Paper 78-144, Jan. 1978.

[12] Hickcox, T., "A Generalized Method of Characteristics (MOCHA) Computer Program for the Solution of Complex Supersonic Two-Dimensional or Axisymmetric Flowfields," The Boeing Co., Doc. D6-41471, 1973.

[13] Hung, C.M. and MacCormack, R.W., "Numerical Solutions of Supersonic and Hypersonic Laminar Flows Over a Two-Dimensional Compression Corner," AIAA Paper 75-2, Jan. 1975.

[14] MacCormack, R.W. and Baldwin, B.S., "A Numerical Method for Solving the Navier-Stokes Equations with Application to Shock-Boundary Layer Interactions," AIAA Paper 75-1, Jan. 1975.

[15] Deiwert, G.S., "Numerical Simulation of High Reynolds Number Transonic Flows," AIAA Paper 74-603, June 1974.

[16] Launder, B.E. and Spalding, D.B., "The Numerical Computation of Turbulent Flows," *Computer Methods in Applied Mechanics and Engineering,* Vol. 3, 1974, pp. 269-289.

[17] MacCormack, R.W. and Paullay, A.J., "The Influence of the Computational Mesh on Accuracy for Initial Value Problems with Discontinuous or Non-Unique Solutions," *Computers and Fluids,* Vol. 2, Pergamon Press, 1974, pp. 339-361.

[18] Schiff, L.B., "The Axisymmetric Jet Counterflow Problem," AIAA Paper 76-325, July 1976.

[19] Thornock, R.L., "Experimental Investigation of the Flow Through Convergent-Conical Nozzles," The Boeing Co., Doc. D6-20375, 1968.

[20] Launder, B.E. and Spalding, D.B., *Mathematical Models of Turbulence,* Academic Press, London and New York, 1972.

[21] Kern, P.R.A., "Wind Tunnel Development of Isolated, Blown Nacelles with Short Duct Fan and Plug Primary Nozzles for the 747 Airplane," The Boeing Co., Doc. D6-13578, 1968.